COMPLEX SYSTEM MODELING AND SIMULATION
ISSN 2096-9929 04/06 pp 220−235
Volume 3, Number 3, September 2023
DOI: 10.23919/CSMS.2023.0010

Comprehensive Model Construction and Simulation for Superconducting Electrodynamic Suspension Train

Linfeng Liu, Hao Ye*, Wei Dong, and Junfeng Cui

Abstract: With the advantages of levitation/guidance self-stability, large levitation gap, and high lift-to-drag ratios, superconducting electrodynamic suspension (SC-EDS) train is becoming a viable candidate for the high-speed and ultra-high-speed rail transportation. In order to provide the basis for designing the optimization and control strategy, this paper establishes a comprehensive model for the SC-EDS train, which considers the dynamics of the bogie and car body in all directions. The obtained model reveals the complex coupling and feedback relationships among the variables, which cannot be described by the existing local models of the SC-EDS train. Simulation examples under different parameters and initial conditions are presented and discussed to demonstrate the potential use of the model given in this paper.

Key words: superconducting electrodynamic suspension train; comprehensive model; coupling and feedback analysis; numerical simulation

1 Introduction

Due to its high speed, high comfort, low energy consumption, and environmental friendliness, the maglev train has been receiving more and more attentions in the research area of rail transportation[1].

Maglev trains can be classified into three types according to their suspension mechanisms[2, 3], i.e., the electromagnetic suspension (EMS) train, the electrodynamic suspension (EDS) train, and the high-temperature superconducting suspension (HTS) train, where the EDS is further divided into two types based on the magnets adopted, i.e., the superconducting magnet based suspension and permanent magnet based suspension[2]. Among the different types of maglev trains, the superconducting electrodynamic suspension (SC-EDS) train has the following advantages: (1) It is self-stable in both levitation and guidance directions[4]; (2) Its largest levitation gap is around 100 mm, much larger than that for the EMS train (10 mm)[2] and the HTS train (15−30 mm)[3], which means a less disturbance from the guideway irregularities; (3) It has high lift-to-drag ratios, high suspension stiffness, and no needs for the expensive permanent magnet guideway required by the HTS train[5]. Therefore, the SC-EDS train has a broad prospect of application in high-speed and ultra-high-speed rail transportation. Actually, only the SC-EDS train has passed the application feasibility verification of 600 km/h speed class[6]. Japan's L0 SC-EDS train has created the highest speed record of 603 km/h in rail transportation[7].

Figure 1 gives a diagram to illustrate the structure of the SC-EDS train and the basic principle for its levitation, guidance, and propulsion[8]. The train is composed of the bogie, the car body, and the secondary suspension connecting them, whose motion is constrained by the guideway. Working as a linear motor, the electromagnetic interaction between the

• Linfeng Liu and Hao Ye are with the Department of Automation, Tsinghua University, Beijing 100084, China. E-mail: llf20@mails.tsinghua.edu.cn; haoye@mail.tsinghua.edu.cn.
• Wei Dong is with the Beijing National Research Center for Information Science and Technology, Tsinghua University, Beijing 100084, China. E-mail: weidong@tsinghua.edu.cn.
• Junfeng Cui is with the CRSC Research & Design Institute Group Co., Ltd, Beijing 100070, China. E-mail: cuijunfeng@crscd.com.cn.
* To whom correspondence should be addressed.
※ This article was recommended by Editor-in-Chief Wenhui Fan. Manuscript received: 2023-04-17; revised: 2023-04-24; accepted: 2023-04-29

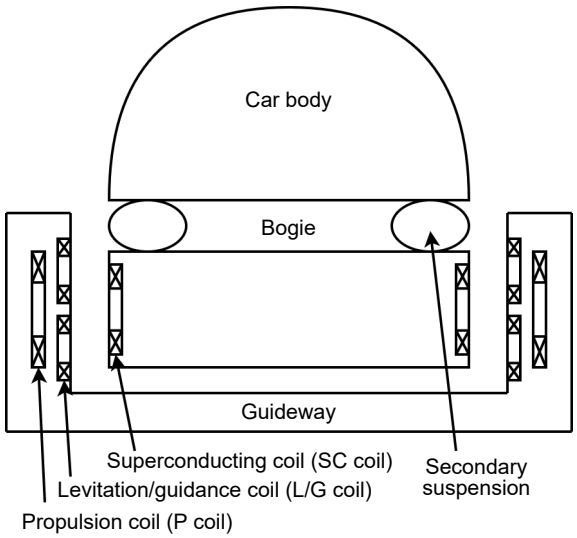

Fig. 1 Layout of the SC-EDS train.

superconducting (SC) coils installed on the bogie and the propulsion coils installed on the guideway produces longitudinal traction/braking force for the train[2]. Then the moving magnetic field produced by the SC coils excites the induced current in the levitation/guidance (L/G) coils installed on the guideway, and the interaction between the moving magnetic field and the induced current further produces vertical levitation force and lateral guidance force for the train[2].

From Fig. 1, it is intuitive that the levitation/guidance force mainly depends on the longitudinal velocity and can not be controlled independently, and there is a complex coupling between the longitudinal dynamics and the vertical/lateral dynamics of the train. So as an indispensable basis for the design of automatic train control system, it is necessary to build a comprehensive model for the SC-EDS train. More specifically, the model should include all of the main components shown in Fig. 1, including car body, bogie, secondary suspension, SC coils, and ground coils, and consider their interactions in all of the six directions, i.e., the longitudinal, vertical, lateral, pitching, rolling, and yawing directions.

The existing research on the modeling of the SC-EDS train can be mainly divided into two classes: (1) the modeling of the electromagnetic forces acting on an SC coil, but without further considering the dynamics of the bogie and the car body; (2) the modeling of the dynamics of the SC-EDS train including the bogie and the car body, but only in the vertical-pitching and lateral-rolling directions.

For the first group of work, based on dynamic circuit theory, Refs. [9−12] calculated the longitudinal, vertical, and lateral electromagnetic forces acting on an SC coil, which is installed on the bogie and interacts with the figure-eight-shaped null flux coil installed on the guideway; Refs. [4, 5, 8, 13−17] extended the model by analyzing the interactions between the SC coil and all of the figure-eight-shaped null flux coils along the entire guideway. A limitation of the above results is that they only focus on the electromagnetic forces acting on the SC coil, but do not consider how it will affect the dynamics of the bogie and car body.

For the second group of work, to improve the vibration damping performance of the SC-EDS train, models for its vertical-pitching and lateral-rolling directions under a given longitudinal velocity are given, respectively[6, 18−24]. In these models, the interaction between the car body and the bogie is further involved, which has not been considered in the first group of work[6, 18−24]. However, only a subset of the six directions (i.e., the longitudinal, vertical, lateral, pitching, rolling, and yawing directions) has been considered in these models. In addition, unlike the first group of work which uses dynamic circuit theory, the second group of work uses linear spring forces to express the electrodynamic forces, which leads to the obtained models less refined.

As for the longitudinal dynamics, there is still lack of research on the SC-EDS train. However, since the traction and braking principles of the SC-EDS train are basically as same as those of the EMS train, the results on longitudinal dynamics modeling of the EMS train[25, 26] are also applicable to the SC-EDS train. The only difference between the two kinds of trains in terms of the longitudinal forces lies in the longitudinal electromagnetic resistance, i.e., the SC-EDS train is subjected to the longitudinal electromagnetic drag force of the L/G coils to the SC coils, while the EMS train is subjected to eddy current resistance generated by the guideway.

Considering the limitation of the existing models for the dynamics of SC-EDS trains, in this paper, we will establish a comprehensive model for the SC-EDS train. The main contributions include: (1) Based on dynamic circuit theory, a non-longitudinal model of the SC-EDS train with 20 degrees of freedom in the five non-longitudinal directions (i.e., the vertical, lateral, pitching, rolling, and yawing directions) is developed, which involves the car body and bogie and takes their interaction in all of the non-longitudinal directions into account. (2) By analyzing the electromagnetic drag force, which is unique to the SC-EDS train, and further

combining it with other longitudinal forces derived from the EMS train, the longitudinal model of the SC-EDS train is established. (3) By combining the non-longitudinal and longitudinal models given in (1) and (2), respectively, a comprehensive model is finally obtained, based on which, a diagram depicting the complex couplings of the car body and the bogie in all directions is given. (4) Simulation examples are given to simulate and analyze the running state and dynamic characteristics of the SC-EDS train under different parameters and conditions, which may play an important role in guiding the design of the SC-EDS train and its optimization and control.

2 Model Structure and Notation

The structure diagram and its three views of the SC-EDS train consisting of a single car body and a single bogie are shown in Fig. 2. In Fig. 2, c, b, and u represent the car body, the bogie, and the guideway, respectively. The car body and the bogie are connected through a secondary suspension consisting of damper d and air spring a in vertical and lateral directions. In the longitudinal direction, the car body and the bogie can be regarded as rigidly connected[23]. r_j (j = 1, 2, 3, 4) and l_j (j = 1, 2, 3, 4) are the eight on-board SC coils (magnets) symmetrically mounted on the right and left sides of the bogie. The car body and the bogie are considered to be rigid. Ground coils including levitation/guidance coils and propulsion coils are mounted on the side wall of the guideway and interact with the SC coils on the bogie to provide the train with the vertical levitation force F_z, the lateral guidance force F_y, and the longitudinal traction/braking force F_x. In Fig. 2, the x, y, and z axes denote the longitudinal, lateral, and vertical directions, respectively, around which, rolling, pitching, and yawing directions can be further defined.

In this paper, we make the following assumptions: (1) The SC-EDS train consists of a single car body and a single bogie; (2) In the longitudinal direction x, we suppose the SC-EDS train adopts the linear synchronous motor in driving, uses the regenerative braking and wheel braking in ordinary braking, and uses the eddy current braking and wheel braking (or skid braking) in emergency braking.

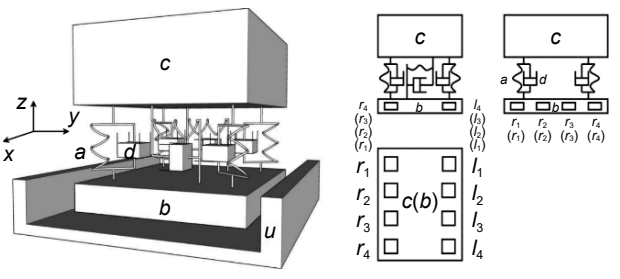

Fig. 2 Structure diagram of the SC-EDS train model.

A main simplification of the model structure compared with the real applications lies in Assumption (1), because the real SC-EDS train usually has multiple car bodies and multiple bogies.

Table 1 lists some key variables involved in the modeling in subsequent sections. In Table 1 and throughout the paper, we use the following notations for the subscript of a variable: (1) x, y, or z denotes the axis with which a variable is associated; (2) r/l denotes the right/left side of the bogie where an SC coil is installed; (3) j = 1, 2, 3, 4 denotes the index number of an SC coil, and (4) b and c denote bogie and car body, respectively. For example, we use $F_{z,r,j}$ to denote the levitation force acting on the SC coil j installed on the right side of bogie and in the vertical direction.

3 Preliminary

This section will give a brief introduction to some important results which will be used in this paper.

3.1 Analysis of the levitation and guidance forces in the SC-EDS train

When the SC-EDS train runs longitudinally, due to the relative motion between the on-board SC coils with strong direct current and the ground coils, an induced current is generated in the ground coils, whose corresponding magnetic field interacts with the magnetic field of the SC coils and further provides levitation/guidance force[5]. Then in a figure-eight-shaped coil system and according to the dynamic circuit theory, the levitation/guidance force acting on the SC coils can be computed according to Eqs. (1)–(4)[4, 5], where the subscript j (for the index number of a specific SC coil) is omitted.

$$\begin{aligned} F_{z,l} = & -\frac{3I_s^2}{4}\frac{1}{L-M}\frac{v_{b,x}^2}{v_{b,x}^2+\beta_1^2}\left[M_{p,l,1}(y_l,z_l)-\right. \\ & \left.M_{p,l,2}(y_l,z_l)\right]\left[\frac{\partial M_{p,l,1}(y_l,z_l)}{\partial z_l}-\frac{\partial M_{p,l,2}(y_l,z_l)}{\partial z_l}\right]- \\ & \frac{3I_s^2}{8}\frac{1}{L+M}\frac{v_{b,x}^2}{v_{b,x}^2+\beta_2^2}\left[M_{p,l,1}(y_l,z_l)+M_{p,l,2}(y_l,z_l)-\right. \\ & \left.M_{p,r,1}(y_r,z_r)-M_{p,r,2}(y_r,z_r)\right]\left[\frac{\partial M_{p,l,1}(y_l,z_l)}{\partial z_l}+\right. \\ & \left.\frac{\partial M_{p,l,2}(y_l,z_l)}{\partial z_l}\right] \end{aligned} \tag{1}$$

Table 1 Definition of key variables in the model.

Variable	Definition
$F_{z,r,j}$ (j = 1, 2, 3, 4) $F_{z,l,j}$ (j = 1, 2, 3, 4)	Levitation forces on the SC coil
$F_{y,r,j}$ (j = 1, 2, 3, 4) $F_{y,l,j}$ (j = 1, 2, 3, 4)	Guidance forces on the SC coil
$W_{x,r,j}$ (j = 1, 2, 3, 4) $W_{x,l,j}$ (j = 1, 2, 3, 4)	Electromagnetic drag forces on the SC coil
W_x	Electromagnetic drag force on the center of mass of the train
$z_{r,j}$ (j = 1, 2, 3, 4) $z_{l,j}$ (j = 1, 2, 3, 4)	Vertical displacements of the center of the SC coil with respect to the center of the ground coil
$y_{r,j}$ (j = 1, 2, 3, 4) $y_{l,j}$ (j = 1, 2, 3, 4)	Lateral displacements of the center of the SC coil with respect to the center of the ground coil
$x_{r,j}$ (j = 1, 2, 3, 4) $x_{l,j}$ (j = 1, 2, 3, 4)	Longitudinal displacements of the center of the SC coil with respect to the center of the ground coil in the current figure-eight-shaped coil system
$z_c, v_{c,z}, a_{c,z}$	Vertical displacement, velocity, and acceleration of the center of mass of the car body
$z_b, v_{b,z}, a_{b,z}$	Vertical displacement, velocity, and acceleration of the center of mass of the bogie
$y_c, v_{c,y}, a_{c,y}$	Lateral displacement, velocity, and acceleration of the center of mass of the car body
$y_b, v_{b,y}, a_{b,y}$	Lateral displacement, velocity, and acceleration of the center of mass of the bogie
$x_c, v_{c,x}, a_{c,x}$	Longitudinal displacement, velocity, and acceleration of the center of mass of the car body
$x_b, v_{b,x}, a_{b,x}$	Longitudinal displacement, velocity, and acceleration of the center of mass of the bogie
$\theta_c, \dot{\theta}_c, \ddot{\theta}_c$	Pitching displacement, velocity, and acceleration of the car body
$\theta_b, \dot{\theta}_b, \ddot{\theta}_b$	Pitching displacement, velocity, and acceleration of the bogie
$\phi_c, \dot{\phi}_c, \ddot{\phi}_c$	Rolling displacement, velocity, and acceleration of the car body
$\phi_b, \dot{\phi}_b, \ddot{\phi}_b$	Rolling displacement, velocity, and acceleration of the bogie
$\varphi_c, \dot{\varphi}_c, \ddot{\varphi}_c$	Yawing displacement, velocity, and acceleration of the car body
$\varphi_b, \dot{\varphi}_b, \ddot{\varphi}_b$	Yawing displacement, velocity, and acceleration of the bogie
F_D	Total traction force
B	Total braking force
W_R	Total resistance except for electromagnetic drag force

$$F_{z,r} = -\frac{3I_s^2}{4}\frac{1}{L-M}\frac{v_{b,x}^2}{v_{b,x}^2+\beta_1^2}\left[M_{p,r,1}(y_r,z_r) - M_{p,r,2}(y_r,z_r)\right]\left[\frac{\partial M_{p,r,1}(y_r,z_r)}{\partial z_r} - \frac{\partial M_{p,r,2}(y_r,z_r)}{\partial z_r}\right] - \frac{3I_s^2}{8}\frac{1}{L+M}\frac{v_{b,x}^2}{v_{b,x}^2+\beta_2^2}\left[M_{p,r,1}(y_r,z_r) + M_{p,r,2}(y_r,z_r) - M_{p,l,1}(y_l,z_l) - M_{p,l,2}(y_l,z_l)\right]\left[\frac{\partial M_{p,r,1}(y_r,z_r)}{\partial z_r} + \frac{\partial M_{p,r,2}(y_r,z_r)}{\partial z_r}\right] \tag{2}$$

$$F_{y,l} = -\frac{3I_s^2}{4}\frac{1}{L-M}\frac{v_{b,x}^2}{v_{b,x}^2+\beta_1^2}\left[M_{p,l,1}(y_l,z_l) - M_{p,l,2}(y_l,z_l)\right]\left[\frac{\partial M_{p,l,1}(y_l,z_l)}{\partial y_l} - \frac{\partial M_{p,l,2}(y_l,z_l)}{\partial y_l}\right] - \frac{3I_s^2}{8}\frac{1}{L+M}\frac{v_{b,x}^2}{v_{b,x}^2+\beta_2^2}\left[M_{p,l,1}(y_l,z_l) + M_{p,l,2}(y_l,z_l) - M_{p,r,1}(y_r,z_r) - M_{p,r,2}(y_r,z_r)\right]\left[\frac{\partial M_{p,l,1}(y_l,z_l)}{\partial y_l} + \frac{\partial M_{p,l,2}(y_l,z_l)}{\partial y_l}\right] \tag{3}$$

$$F_{y,r} = -\frac{3I_s^2}{4}\frac{1}{L-M}\frac{v_{b,x}^2}{v_{b,x}^2+\beta_1^2}\left[M_{p,r,1}(y_r,z_r) - M_{p,r,2}(y_r,z_r)\right]\left[\frac{\partial M_{p,r,1}(y_r,z_r)}{\partial y_r} - \frac{\partial M_{p,r,2}(y_r,z_r)}{\partial y_r}\right] - \frac{3I_s^2}{8}\frac{1}{L+M}\frac{v_{b,x}^2}{v_{b,x}^2+\beta_2^2}\left[M_{p,r,1}(y_r,z_r) + M_{p,r,2}(y_r,z_r) - M_{p,l,1}(y_l,z_l) - M_{p,l,2}(y_l,z_l)\right]\left[\frac{\partial M_{p,r,1}(y_r,z_r)}{\partial y_r} + \frac{\partial M_{p,r,2}(y_r,z_r)}{\partial y_r}\right] \tag{4}$$

In Eqs. (1)–(4), $\beta_1 = \tau R/\pi(L-M)$, $\beta_2 = \tau R/\pi(L+M)$, I_s is the current in the SC coil, τ is the pole pitch of the SC coil, R is the equivalent resistance of the ground coil, L is the equivalent inductance of the ground coil, M is the mutual inductance coefficient between upper and lower ground coils, $M_{p,l,i}/M_{p,r,i}$ is the mutual inductance coefficient between the SC coils and the ground coils on the r/l side of the guideway when they coincide in longitudinal center, and subscript i = 1, 2 denotes the upper and lower ground coils, respectively. Please refer to Refs. [4, 5] for the calculation of $M_{p,l,i}/M_{p,r,i}$.

Remark 1 Equations (1)–(4) give a model for the levitation/guidance force acting on an SC coil, where the motion states of the SC coil (including the vertical displacements z_l and z_r, lateral displacements y_l and y_r,

and longitudinal velocity $v_{b,x}$) are input variables, and the levitation/guidance forces $F_{z,l}$, $F_{z,r}$, $F_{y,l}$, and $F_{y,r}$ acting on the SC coils are output variables.

3.2 Equivalent current in the ground coil

As a basis in the modeling of the levitation/guidance force on the SC coil, Ref. [5] also obtains the equivalent currents of the ground coils in a figure-eight-shaped coil system, i.e., Eqs. (5)–(7)[5].

$$i_1 = \frac{\omega I_s\left(M_{p,l,1} - M_{p,l,2}\right)}{2\sqrt{R^2 + \omega^2(L-M)^2}}\sin(\omega t - \alpha_1) + \frac{1}{2}i_2 \tag{5}$$

$$i_2 = \frac{\omega I_s\left(M_{p,l,1} + M_{p,l,2} - M_{p,r,1} - M_{p,r,2}\right)}{2\sqrt{R^2 + \omega^2(L+M)^2}}\sin(\omega t - \alpha_2) \tag{6}$$

$$i_3 = \frac{\omega I_s\left(M_{p,r,1} - M_{p,r,2}\right)}{2\sqrt{R^2 + \omega^2(L-M)^2}}\sin(\omega t - \alpha_1) + \frac{1}{2}i_2 \tag{7}$$

where $\alpha_1 = \tan^{-1}(\omega(L-M)/R)$, $\alpha_2 = \tan^{-1}(\omega(L-M)/R)$, $\omega = \pi v_{b,x}/\tau$, and i_j (j = 1, 2, 3) represents the equivalent currents of each circuit in the equivalent circuit shown in Fig. 3.

3.3 Analysis of the longitudinal forces in the EMS train

The EMS train is mainly affected by three kinds of forces in the longitudinal direction during operation, which are traction force, braking force, and resistance[25, 26]. The traction force includes the traction force from linear synchronous motor F_x and the slope sliding force F_I when downhill. The braking force includes the regenerative braking force B_R (i.e., the force generated by the reversal of the linear synchronous motor), the eddy current braking force B_E, the skid braking force B_S, and the wheel braking force B_W. The resistance includes the slope sliding force

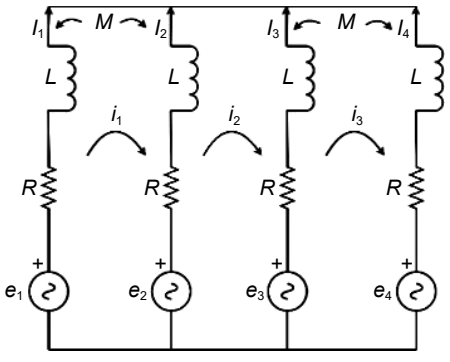

Fig. 3 Equivalent circuit of the ground coils in the figure-eight-shaped coil system.

when uphill, the air resistance W_A, the resistance caused by the DC generator W_B, and the eddy current resistance[25, 26]. The following Eqs. (8)–(15) list how to calculate these forces in the EMS train[25, 26] except the eddy current resistance.

$$F_x = \frac{3\pi}{2\tau_l}\left(\Psi_d i_q - \Psi_q i_d\right) \doteq nK_p I_D \tag{8}$$

$$F_I = \frac{mgi}{1000} \tag{9}$$

$$B_R = \frac{3\pi}{2\tau}\left(\Psi_d i_q - \Psi_q i_d\right) \tag{10}$$

$$B_E = q_E 1.2m\left(1 - \mathrm{e}^{-\frac{v}{v_0}}\right) \tag{11}$$

$$B_S = \mu_S mg\sqrt{1 - (i/1000)^2} \tag{12}$$

$$B_W = q_W \mu_W F_0 \tag{13}$$

$$W_A = 0.5P_L C_X S_F\left(\frac{0.6n}{2} + 0.4\right)v^2 \tag{14}$$

$$W_B = \begin{cases} 0, & v = 0; \\ 3.3n, & 0 < v < v_1; \\ n\left(\dfrac{146}{v} - 0.2\right), & v \geqslant v_1 \end{cases} \tag{15}$$

where τ_l is the pole pitch of the linear synchronous motor, i_d and i_q are the current components of the stator windings in the *d-q-o* coordinate system, Ψ_d and Ψ_q are the flux components of the stator windings in the *d-q-o* coordinate system, n is the number of train cars in the marshalling, equaling 1 in the model in this paper, K_p is the thrust coefficient of single train car, I_D is the effective value of stator current, m is the weight of train, i.e., $m_c + m_b$ in this paper, g is gravitational acceleration, assuming that the guideway slope is i‰, q_E is the class of eddy current brake, v_0 is the velocity constant, μ_S is the friction coefficient, q_W is the class of wheel braking, μ_W is the wheel friction coefficient, F_0 is the maximum pressure from the wheel, v is the longitudinal velocity of the train, P_L is the air density, C_X is the air damping coefficient, S_F is the area of the front of the train, and v_1 is the critical speed at which a generator operates.

It is worth mentioning that most of the above models also apply to the SC-EDS train. Actually, the only difference between the SC-EDS train and the EMS train with respect to the longitudinal forces is in the resistance, i.e., the EMS train is subjected to the eddy current resistance of the guideway, while the SC-EDS

train is subjected to the electromagnetic drag force on SC coils. So for SC-EDS train, the electromagnetic drag force will be analyzed in the next section of this paper.

4 Comprehensive Model of the SC-EDS Train

4.1 Non-longitudinal dynamics

Based on Newton-Euler equation and the force/moment balance analysis, the dynamics of the car body and bogie of the SC-EDS train (see Fig. 2) are given in Eqs. (16)–(25), which are the vertical force balance equation of the center of mass of the bogie, the vertical force balance equation of the center of mass of the car body, the lateral force balance equation of the center of mass of the bogie, the lateral force balance equation of the center of mass of the car body, the pitching moment balance equation of the bogie, the pitching moment balance equation of the car body, the rolling moment balance equation of the bogie, the rolling moment balance equation of the car body, the yawing moment balance equation of the bogie, and the yawing moment balance equation of the car body, respectively.

$$-m_b g + F_{z,r,1} + F_{z,r,2} + F_{z,r,3} + F_{z,r,4} + F_{z,l,1} + F_{z,l,2} + F_{z,l,3} + F_{z,l,4} - 4k_z z_b - 4c_z v_{b,z} + 4k_z z_c + 4c_z v_{c,z} = m_b a_{b,z} \quad (16)$$

$$-m_c g - 4k_z z_c - 4c_z v_{c,z} + 4k_z z_b + 4c_z v_{b,z} = m_c a_{c,z} \quad (17)$$

$$F_{y,r,1} + F_{y,r,2} + F_{y,r,3} + F_{y,r,4} + F_{y,l,1} + F_{y,l,2} + F_{y,l,3} + F_{y,l,4} - 4k_y y_b - 4c_y v_{b,y} + 4k_y y_c + 4c_y v_{c,y} = m_b a_{b,y} \quad (18)$$

$$-4k_y y_c - 4c_y v_{c,y} + 4k_y y_b + 4c_y v_{b,y} = m_c a_{c,y} \quad (19)$$

$$F_{z,r,1} l_{x,1} + F_{z,r,2} l_{x,2} + F_{z,l,1} l_{x,1} + F_{z,l,2} l_{x,2} - F_{z,r,3} l_{x,2} - F_{z,r,4} l_{x,1} - F_{z,l,3} l_{x,2} - F_{z,l,4} l_{x,1} - 4k_z l_{x,1}^2 \theta_b - 4c_z l_{x,1}^2 \dot{\theta}_b + 4k_z l_{x,1}^2 \theta_c + 4c_z l_{x,1}^2 \dot{\theta}_c = I_{b,\theta} \ddot{\theta}_b \quad (20)$$

$$-4k_z l_{x,1}^2 \theta_c - 4c_z l_{x,1}^2 \dot{\theta}_c + 4k_z l_{x,1}^2 \theta_b + 4c_z l_{x,1}^2 \dot{\theta}_b = I_{c,\theta} \ddot{\theta}_c \quad (21)$$

$$F_{z,l,1} l_y + F_{z,l,2} l_y + F_{z,l,3} l_y + F_{z,l,4} l_y - F_{z,r,1} l_y + F_{z,r,2} l_y - F_{z,r,3} l_y - F_{z,r,4} l_y - 4k_z l_y^2 \phi_b - 4c_z l_y^2 \dot{\phi}_b + 4k_z l_y^2 \phi_c + 4c_z l_y^2 \dot{\phi}_c = I_{b,\phi} \ddot{\phi}_b \quad (22)$$

$$-4k_z l_y^2 \phi_c - 4c_z l_y^2 \dot{\phi}_c + 4k_z l_y^2 \phi_b + 4c_z l_y^2 \dot{\phi}_b = I_{c,\phi} \ddot{\phi}_c \quad (23)$$

$$F_{y,r,3} l_{x,2} + F_{y,r,4} l_{x,1} + F_{y,l,3} l_{x,2} + F_{y,l,4} l_{x,1} - F_{y,r,1} l_{x,1} - F_{y,r,2} l_{x,2} - F_{y,l,1} l_{x,1} - F_{y,l,2} l_{x,2} - 4k_y l_{x,1}^2 \varphi_b - 4c_y l_{x,1}^2 \dot{\varphi}_b + 4k_y l_{x,1}^2 \varphi_c + 4c_y l_{x,1}^2 \dot{\varphi}_c = I_{b,\varphi} \ddot{\varphi}_b \quad (24)$$

$$-4k_y l_{x,1}^2 \varphi_c - 4c_y l_{x,1}^2 \dot{\varphi}_c + 4k_y l_{x,1}^2 \varphi_b + 4c_y l_{x,1}^2 \dot{\varphi}_b = I_{c,\varphi} \ddot{\varphi}_c \quad (25)$$

In Eqs. (16)–(25), besides the variables defined in Table 1, m_b and m_c are the weights of the bogie and the car body, $I_{b,\theta}$, $I_{b,\phi}$, and $I_{b,\varphi}$ are the pitching, rolling, and yawing inertia moments of the bogie, $I_{c,\theta}$, $I_{c,\phi}$, and $I_{c,\varphi}$ are the pitching, rolling, and yawing inertia moments of the car body, k_z and k_y are the vertical and lateral air spring stiffness, c_z and c_y are the damping coefficients of the vertical and lateral dampers, $l_{x,1}$ and $l_{x,2}$ are the longitudinal distances between the center of mass of the bogie (car body) and the outer and inner SC coils, respectively, and l_y is the lateral distance between the center of mass of the bogie (car body) and the SC coil.

In Eqs. (16)–(25), the levitation/guidance forces on the SC coils, i.e., $F_{z,r,j}, F_{z,l,j}, F_{y,r,j}$, and $F_{y,l,j}$ (j = 1, 2, 3, 4) can be calculated by Eqs. (1)–(4), in which the subscript j (for the index number of a specific SC coil) is omitted.

Equations (16)–(25) can be written in the following matrix form:

$$G\ddot{X}_0 = N\dot{X}_0 + PX_0 + QF + K \quad (26)$$

where $X_0 \in R^{10\times 1} = [z_b\ z_c\ y_b\ y_c\ \theta_b\ \theta_c\ \phi_b\ \phi_c\ \varphi_b\ \varphi_c]^{\mathrm{T}}$ and $F \in R^{16\times 1} = [F_{z,r,1}\ F_{z,r,2}\ F_{z,r,3}\ F_{z,r,4}\ F_{z,l,1}\ F_{z,l,2}\ F_{z,l,3}\ F_{z,l,4}\ F_{y,r,1}\ F_{y,r,2}\ F_{y,r,3}\ F_{y,r,4}\ F_{y,l,1}\ F_{y,l,2}\ F_{y,l,3}\ F_{y,l,4}]^{\mathrm{T}}$ represent the displacement vector and the levitation/guidance forces vector, respectively. The details of the matrixes G, N, P, Q, and K are given in Eqs. (27)–(31).

$$G = \begin{bmatrix} m_b & & & & & & & & & \\ & m_c & & & & & & & & \\ & & m_b & & & & & & & \\ & & & m_c & & & & & & \\ & & & & I_{b,\theta} & & & & & \\ & & & & & I_{c,\theta} & & & & \\ & & & & & & I_{b,\phi} & & & \\ & & & & & & & I_{c,\phi} & & \\ & & & & & & & & I_{b,\varphi} & \\ & & & & & & & & & I_{c,\varphi} \end{bmatrix} \quad (27)$$

$$N=\begin{bmatrix}
-4c_z & 4c_z & & & & & & & & & & & & & & \\
4c_z & -4c_z & & & & & & & & & & & & & & \\
 & & -4c_y & 4c_y & & & & & & & & & & & & \\
 & & 4c_y & -4c_y & & & & & & & & & & & & \\
 & & & & -4c_z l_{x,1}^2 & 4c_z l_{x,1}^2 & & & & & & & & & & \\
 & & & & 4c_z l_{x,1}^2 & -4c_z l_{x,1}^2 & & & & & & & & & & \\
 & & & & & & -4c_z l_y^2 & 4c_z l_y^2 & & & & & & & & \\
 & & & & & & 4c_z l_y^2 & -4c_z l_y^2 & & & & & & & & \\
 & & & & & & & & -4c_y l_{x,1}^2 & 4c_y l_{x,1}^2 & & & & & & \\
 & & & & & & & & 4c_y l_{x,1}^2 & -4c_y l_{x,1}^2 & & & & & &
\end{bmatrix} \tag{28}$$

$$P=\begin{bmatrix}
-4k_z & 4k_z & & & & & & & & & & & & & & \\
4k_z & -4k_z & & & & & & & & & & & & & & \\
 & & -4k_y & 4k_y & & & & & & & & & & & & \\
 & & 4k_y & -4k_y & & & & & & & & & & & & \\
 & & & & -4k_z l_{x,1}^2 & 4k_z l_{x,1}^2 & & & & & & & & & & \\
 & & & & 4k_z l_{x,1}^2 & -4k_z l_{x,1}^2 & & & & & & & & & & \\
 & & & & & & -4k_z l_y^2 & 4k_z l_y^2 & & & & & & & & \\
 & & & & & & 4k_z l_y^2 & -4k_z l_y^2 & & & & & & & & \\
 & & & & & & & & -4k_y l_{x,1}^2 & 4k_y l_{x,1}^2 & & & & & & \\
 & & & & & & & & 4k_y l_{x,1}^2 & -4k_y l_{x,1}^2 & & & & & &
\end{bmatrix} \tag{29}$$

$$Q=\begin{bmatrix}
1 & 1 & 1 & 1 & 1 & 1 & 1 & 1 & 0 & 0 & 0 & 0 & 0 & 0 & 0 & 0 \\
0 & 0 & 0 & 0 & 0 & 0 & 0 & 0 & 0 & 0 & 0 & 0 & 0 & 0 & 0 & 0 \\
0 & 0 & 0 & 0 & 0 & 0 & 0 & 0 & 1 & 1 & 1 & 1 & 1 & 1 & 1 & 1 \\
0 & 0 & 0 & 0 & 0 & 0 & 0 & 0 & 0 & 0 & 0 & 0 & 0 & 0 & 0 & 0 \\
l_{x,1} & l_{x,2} & -l_{x,2} & -l_{x,1} & l_{x,1} & l_{x,2} & -l_{x,2} & -l_{x,1} & 0 & 0 & 0 & 0 & 0 & 0 & 0 & 0 \\
0 & 0 & 0 & 0 & 0 & 0 & 0 & 0 & 0 & 0 & 0 & 0 & 0 & 0 & 0 & 0 \\
l_y & l_y & l_y & l_y & l_y & l_y & l_y & l_y & 0 & 0 & 0 & 0 & 0 & 0 & 0 & 0 \\
0 & 0 & 0 & 0 & 0 & 0 & 0 & 0 & 0 & 0 & 0 & 0 & 0 & 0 & 0 & 0 \\
0 & 0 & 0 & 0 & 0 & 0 & 0 & 0 & -l_{x,1} & -l_{x,2} & l_{x,2} & l_{x,1} & -l_{x,1} & -l_{x,2} & l_{x,2} & l_{x,1} \\
0 & 0 & 0 & 0 & 0 & 0 & 0 & 0 & 0 & 0 & 0 & 0 & 0 & 0 & 0 & 0
\end{bmatrix} \tag{30}$$

$$K=[-m_b g\ -m_c g\ 0\ 0\ 0\ 0\ 0\ 0\ 0\ 0]^{\mathrm{T}} \tag{31}$$

Remark 2 Equations (16)–(25) (or Eq. (26) in matrix form) describe how the levitation/guidance forces F acting on the SC coils affect the motion states X_0 of the car body and bogie in non-longitudinal directions (including the vertical, lateral, pitching, rolling, and yawing directions). While from Eqs. (1)–(4), it can be seen that the forces F further rely on the vertical and lateral displacements $z_{r,j}, z_{l,j}, y_{r,j}$, and $y_{l,j}$ (j = 1, 2, 3, 4), and the longitudinal velocity $v_{b,x}$ of the SC coils on the bogie. It is intuitive that the vertical displacements of the SC coils $z_{r,j}$ and $z_{l,j}$ (j = 1, 2, 3, 4) depend on the vertical displacement z_b, pitching displacement θ_b, and rolling displacement ϕ_b of the bogie, and $y_{r,j}$ and $y_{l,j}$ (j = 1, 2, 3, 4) rely on the lateral displacement y_b and the yawing displacement φ_b of the bogie. This implies a feedback of the motion states $z_b, y_b, \theta_b, \phi_b$, and φ_b to the levitation/guidance forces F. So Eqs. (16)–(25) together with Eqs. (1)–(4) show the complex coupling and feedback among the motions of the car body and the bogie in all non-longitudinal directions, which have not been considered in the existing relevant research.

Remark 3 Equations (1)–(4) and (26) not only reveal the dynamics of the bogie and car body in the vertical, lateral, pitching, rolling, and yawing

directions, but also show how the longitudinal speed $v_{b,x}$ affects the non-longitudinal motion states of the train, which makes the control of SC-EDS train more difficult than EMS train.

Let $X_{11} = \dot{X}_0$, $X_{12} = X_0$, and $X_1 = \left[X_{12}^{\mathrm{T}}\ X_{11}^{\mathrm{T}}\right]^{\mathrm{T}}$. Then Eq. (26) can be written into a state-space equation for the optimization and control problems, i.e.,

$$\dot{X}_1 = A_1 X_1 + B_1 F(X_1, v_{b,x}) + C_1 K \tag{32}$$

where $X_1 \in R^{20\times 1} = [z_b\ z_c\ y_b\ y_c\ \theta_b\ \theta_c\ \phi_b\ \phi_c\ \varphi_b\ \varphi_c\ v_{b,z}\ v_{c,z}\ v_{b,y}\ v_{c,y}\ \dot{\theta}_b\ \dot{\theta}_c\ \dot{\phi}_b\ \dot{\phi}_c\ \dot{\varphi}_b\ \dot{\varphi}_c]^{\mathrm{T}}$ represents the state variable, $A_1 = \begin{bmatrix} 0 & I \\ G^{-1}P & G^{-1}N \end{bmatrix} \in R^{20\times 20}$, $B_1 = \begin{bmatrix} 0 \\ G^{-1}Q \end{bmatrix} \in R^{20\times 16}$, and $C_1 = \begin{bmatrix} 0 \\ G^{-1} \end{bmatrix} \in R^{20\times 10}$.

4.2 Longitudinal dynamics

As mentioned in Section 3.3, except the electromagnetic drag force which exists in the SC-EDS train as a resistance, all the longitudinal force models for the EMS train given in Section 3.3 are also applicable to the SC-EDS train. So in this section, we first analyze the longitudinal electromagnetic drag force on the SC-EDS train based on dynamic circuit theory and the conclusions on equivalent currents[5] given in Section 3.2, and then combine the obtained model of electromagnetic drag force and the other longitudinal force models given in Section 3.3 to give the final longitudinal model for the SC-EDS train.

4.2.1 Analysis of the electromagnetic drag force

According to Ref. [5], the mutual inductance coefficient between SC coil and ground coil can be written as

$$M_{s,j}(x_0, y_0, z_0) = M_{p,j}(y_0, z_0)\cos(\omega t) \tag{33}$$

Substituting Eq. (33) into Eqs. (5)–(7) and considering the relationship between the currents in the equivalent circuit shown in Fig. 3, it can be concluded that the current of each branch in the equivalent circuit I_j (j = 1, 2, 3, 4) can be given by Eqs. (34)–(37).

$$I_1 = \frac{\omega I_s (M_{s,l,1} - M_{s,l,2})}{2\sqrt{R^2 + \omega^2 (L-M)^2}} \frac{\sin(\omega t - \alpha_1)}{\cos(\omega t)} + \frac{\omega I_s (M_{s,l,1} + M_{s,l,2} - M_{s,r,1} - M_{s,r,2})}{4\sqrt{R^2 + \omega^2 (L+M)^2}} \frac{\sin(\omega t - \alpha_2)}{\cos(\omega t)} \tag{34}$$

$$I_2 = -\frac{\omega I_s (M_{s,l,1} - M_{s,l,2})}{2\sqrt{R^2 + \omega^2 (L-M)^2}} \frac{\sin(\omega t - \alpha_1)}{\cos(\omega t)} + \frac{\omega I_s (M_{s,l,1} + M_{s,l,2} - M_{s,r,1} - M_{s,r,2})}{4\sqrt{R^2 + \omega^2 (L+M)^2}} \frac{\sin(\omega t - \alpha_2)}{\cos(\omega t)} \tag{35}$$

$$I_3 = \frac{\omega I_s (M_{s,r,1} - M_{s,r,2})}{2\sqrt{R^2 + \omega^2 (L-M)^2}} \frac{\sin(\omega t - \alpha_1)}{\cos(\omega t)} - \frac{\omega I_s (M_{s,l,1} + M_{s,l,2} - M_{s,r,1} - M_{s,r,2})}{4\sqrt{R^2 + \omega^2 (L+M)^2}} \frac{\sin(\omega t - \alpha_2)}{\cos(\omega t)} \tag{36}$$

$$I_4 = -\frac{\omega I_s (M_{s,r,1} - M_{s,r,2})}{2\sqrt{R^2 + \omega^2 (L-M)^2}} \frac{\sin(\omega t - \alpha_1)}{\cos(\omega t)} - \frac{\omega I_s (M_{s,l,1} + M_{s,l,2} - M_{s,r,1} - M_{s,r,2})}{4\sqrt{R^2 + \omega^2 (L+M)^2}} \frac{\sin(\omega t - \alpha_2)}{\cos(\omega t)} \tag{37}$$

where $M_{s,l,i}/M_{s,r,i}$ is the mutual inductance coefficient between the SC coil and the ground coils on the r/l side of the guideway, and subscript i = 1, 2 denotes the upper and lower ground coils, respectively. Please refer to Refs. [4, 5] for the calculation of $M_{s,l,i}/M_{s,r,i}$.

By using the energy method[4, 5], the longitudinal electromagnetic drag force acting on the SC coil from the ground coils $f_{x,l}$ and $f_{x,r}$ can be given by Eqs. (38) and (39), i.e.,

$$f_{x,l} = I_s I_1 \frac{\partial M_{s,l,1}}{\partial x_l} + I_s I_2 \frac{\partial M_{s,l,2}}{\partial x_l} = \frac{\omega I_s^2 (M_{s,l,1} - M_{s,l,2})}{2\sqrt{R^2 + \omega^2 (L-M)^2}} \frac{\sin(\omega t - \alpha_1)}{\cos(\omega t)} \left(\frac{\partial M_{s,l,1}}{\partial x_l} - \frac{\partial M_{s,l,2}}{\partial x_l}\right) + \frac{\omega I_s^2 (M_{s,l,1} + M_{s,l,2} - M_{s,r,1} - M_{s,r,2})}{4\sqrt{R^2 + \omega^2 (L+M)^2}} \frac{\sin(\omega t - \alpha_2)}{\cos(\omega t)} \cdot \left(\frac{\partial M_{s,l,1}}{\partial x_l} + \frac{\partial M_{s,l,2}}{\partial x_l}\right) \tag{38}$$

$$f_{x,r} = I_s I_1 \frac{\partial M_{s,l,1}}{\partial x_r} + I_s I_2 \frac{\partial M_{s,l,2}}{\partial x_r} = \frac{\omega I_s^2 (M_{s,l,1} - M_{s,l,2})}{2\sqrt{R^2 + \omega^2 (L-M)^2}} \frac{\sin(\omega t - \alpha_1)}{\cos(\omega t)} \left(\frac{\partial M_{s,l,1}}{\partial x_r} - \frac{\partial M_{s,l,2}}{\partial x_r}\right) + \frac{\omega I_s^2 (M_{s,l,1} + M_{s,l,2} - M_{s,r,1} - M_{s,r,2})}{4\sqrt{R^2 + \omega^2 (L+M)^2}} \frac{\sin(\omega t - \alpha_2)}{\cos(\omega t)} \cdot \left(\frac{\partial M_{s,l,1}}{\partial x_r} + \frac{\partial M_{s,l,2}}{\partial x_r}\right) \tag{39}$$

According to the experimental data of Yamanashi test line, the pole pitch of the SC coil is always three times the pole pitch of the ground coil[16, 17], which is equivalent to the situation that an SC coil is subjected to the electromagnetic forces of three neighbor sets of ground coils at a certain time[5]. According to Refs. [5, 17], the phase difference of the three electromagnetic forces is $\tau/3v_{b,x}$. So finally, the longitudinal electromagnetic drag force can be obtained as follows by summing the three forces and averaging them in time.

$$
\begin{aligned}
W_{x,l} = & -\frac{3I_s^2}{2}\frac{1}{L-M}\frac{v_{b,x}^2}{v_{b,x}^2+\beta_1^2}\left[M_{s,l,1}(x_l,y_l,z_l)-\right.\\
& \left.M_{s,2}(x_l,y_l,z_l)\right]\left[\frac{\partial M_{s,l,1}(x_l,y_l,z_l)}{\partial x_l}-\right.\\
& \left.\frac{\partial M_{s,l,2}(x_l,y_l,z_l)}{\partial x_l}\right]-\\
& \frac{3I_s^2}{4}\frac{1}{L+M}\frac{v_{b,x}^2}{v_{b,x}^2+\beta_2^2}\left[M_{s,l,1}(x_l,y_l,z_l)+\right.\\
& \left.M_{s,l,2}(x_l,y_l,z_l)-M_{s,r,1}(x_r,y_r,z_r)-\right.\\
& \left.M_{s,r,2}(x_r,y_r,z_r)\right]\left[\frac{\partial M_{s,l,1}(x_l,y_l,z_l)}{\partial x_l}+\right.\\
& \left.\frac{\partial M_{s,l,2}(x_l,y_l,z_l)}{\partial x_l}\right]
\end{aligned}
\tag{40}
$$

$$
\begin{aligned}
W_{x,r} = & -\frac{3I_s^2}{2}\frac{1}{L-M}\frac{v_{b,x}^2}{v_{b,x}^2+\beta_1^2}\left[M_{s,r,1}(x_r,y_r,z_r)-\right.\\
& \left.M_{s,r,2}(x_r,y_r,z_r)\right]\left[\frac{\partial M_{s,r,1}(x_r,y_r,z_r)}{\partial x_r}-\right.\\
& \left.\frac{\partial M_{s,r,2}(x_r,y_r,z_r)}{\partial x_r}\right]-\\
& \frac{3I_s^2}{4}\frac{1}{L+M}\frac{v_{b,x}^2}{v_{b,x}^2+\beta_2^2}\left[M_{s,r,1}(x_r,y_r,z_r)+\right.\\
& \left.M_{s,r,2}(x_r,y_r,z_r)-M_{s,l,1}(x_l,y_l,z_l)-\right.\\
& \left.M_{s,l,2}(x_l,y_l,z_l)\right]\left[\frac{\partial M_{s,r,1}(x_r,y_r,z_r)}{\partial x_r}+\right.\\
& \left.\frac{\partial M_{s,r,2}(x_r,y_r,z_r)}{\partial x_r}\right]
\end{aligned}
\tag{41}
$$

Remark 4 In Eqs. (40) and (41), the input variables are the longitudinal displacements x_l and x_r, vertical displacements z_l and z_r, lateral displacements y_l and y_r, and longitudinal velocity $v_{b,x}$ of the SC coils. The output variables are the longitudinal electromagnetic drag forces $F_{x,l}$ and $F_{x,r}$ on the SC coils. So Eqs. (40) and (41) show how the motion states $x_l, x_r, z_l, z_r, y_l, y_r$, and $v_{b,x}$ affect the longitudinal electromagnetic drag force on the SC coil.

According to the structure of the SC-EDS train shown in Fig. 2, the electromagnetic drag force of the train can be written as

$$
\begin{aligned}
W_x = & W_{x,l,1}+W_{x,l,2}+W_{x,l,3}+W_{x,l,4}+\\
& W_{x,r,1}+W_{x,r,2}+W_{x,r,3}+W_{x,r,4}
\end{aligned}
\tag{42}
$$

4.2.2 Longitudinal model

The resultant force on the train in the longitudinal direction is given by

$$
\begin{aligned}
F_t = & F_x+F_I-B_R-B_W-B_E-\\
& B_S-W_A-W_B-W_I-W_X
\end{aligned}
\tag{43}
$$

Define the total traction force of the train as F_D, the total braking force as B, the other resistance except the electromagnetic drag force as W_R, and the electromagnetic drag force as W_x. The longitudinal model of the SC-EDS train can be written as

$$
\begin{cases}
\dot{s} = v, \\
\dot{v} = a = \dfrac{F_{\mathrm{D}}-W_R-W_x-B}{m_b+m_c}
\end{cases}
\tag{44}
$$

where s and v represent the longitudinal displacement and velocity of the center of mass of the train, respectively. Since the car body and the bogie are assumed to be rigidly connected in the longitudinal direction, there are $s = x_b = x_c$ and $v = v_{b,x} = v_{c,x}$.

Define $X_2 = [s\ v]^{\mathrm{T}}$ as the state variable and $U = [F_D\ B]^{\mathrm{T}}$ as the input variable. Then the longitudinal model can be written into the following matrix form

$$
\dot{X}_2 = A_2X_2 + B_2U + W_2 + W_{x2} \tag{45}
$$

where $A_2 = \begin{bmatrix} 0 & 1 \\ 0 & 0 \end{bmatrix}$, $B_2 = \begin{bmatrix} 0 & 0 \\ \dfrac{1}{m_b+m_c} & -\dfrac{1}{m_b+m_c} \end{bmatrix}$, $W_2 = \begin{bmatrix} 0 \\ -\dfrac{W_R}{m_b+m_c} \end{bmatrix} = \begin{bmatrix} 0 \\ \dfrac{-W_A-W_B-W_I}{m_b+m_c} \end{bmatrix}$, and $W_{x2} = \begin{bmatrix} 0 \\ -\dfrac{W_x}{m_b+m_c} \end{bmatrix}$.

W_{x2} and W_2 represent the matrix of the electromagnetic drag force and the matrix of other resistance, respectively. From Eqs. (40) and (41), there is a nonlinear relationship between the electromagnetic drag force and the velocity v in the state variable and other parameters such as the lateral and vertical displacements of the SC coils. From Eqs. (14) and (15), W_2 also has a nonlinear relationship with the state variable.

Remark 5 The longitudinal model of the SC-EDS train expressed in Eq. (45) not only considers the longitudinal dynamics of the train but also considers the coupling between the dynamics of longitudinal direction and other directions. It can be seen from Eqs. (40) and (41) that the electromagnetic drag force on the train has a complex nonlinear relationship with the longitudinal displacement, vertical displacement, lateral displacement, and longitudinal velocity of the SC coils on the bogie, and the longitudinal, vertical, and lateral displacements of the SC coils are related to the displacements and attitude angles of the bogie. Therefore, there is a complex coupling between the longitudinal model expressed in Eq. (45) and the dynamics in the other non-longitudinal directions.

4.3 Comprehensive model

Combining the non-longitudinal model and the longitudinal model given in Sections 4.1 and 4.2, respectively, and defining the state variable as $X = \left[X_1^{\mathrm{T}}\ X_2^{\mathrm{T}}\right]^{\mathrm{T}}$, we can finally get the comprehensive model for the SC-EDS train, i.e.,

$$\dot{X} = A_0 X + B_0 U + C_0 F + D_0 W + E_0 K \tag{46}$$

where $A_0 = \begin{bmatrix} A_1 & 0 \\ 0 & A_2 \end{bmatrix}$, $B_0 = \begin{bmatrix} 0 \\ B_2 \end{bmatrix}$, $C_0 = \begin{bmatrix} B_1 \\ 0 \end{bmatrix}$, $D_0 = \begin{bmatrix} 0 \\ I \end{bmatrix}$, and $E_0 = \begin{bmatrix} C_1 \\ 0 \end{bmatrix}$.

The comprehensive model of the SC-EDS train considers the motions of the train in all directions (including longitudinal, vertical, lateral, pitching, rolling, and yawing directions) and the complex coupling and feedback relationships among them. In this model, the input variable is the traction/braking force of the train U, the output variable (state variable) is the motion state (displacement, velocity, and acceleration) of the car body and the bogie, the variables F and W are both determined by the motion states X according to Eqs. (1)–(4), (14), (15), (40), and (41) and affected by the input variable U, and K is the constant term.

Based on Eq. (46), we can plot a system diagram in Fig. 4 for the comprehensive SC-EDS train model established in this paper, which shows the coupling and feedback relationships (which are marked in red color) among the variables more clearly.

5 Simulation

In this section, to show the potential use of the comprehensive model established in Section 4, simulation examples based on it under different parameters and initial conditions will be presented and discussed. The simulation is performed on Matlab.

5.1 Experiment setup

In the simulation, the parameters of the Japanese MLX01 EDS train are adopted and listed in Table 2[5, 19].

As in Ref. [23], random disturbances are added to simulate the guideway irregularities and traction/braking force uncertainty. Specifically, the vertical and lateral guideway irregularities with the power spectral density $S(f) = Ef^{-k}$ is added[22], where E is the guideway roughness constant and set to 0.02 in this paper, f is the spatial domain frequency, and k is the wave number and set to 1.8 in this paper[23]. The traction/braking force of the linear synchronous motor is calculated according to Eq. (8), and a random disturbance signal with zero mean and normal distribution is added.

Motions of the train under three scenarios are considered: (1) uniform movement in the longitudinal direction with different initial heights of the bogie and car body, (2) uniform movement in the longitudinal direction with different stiffness of the lateral air springs and different lateral damping coefficients, and (3) braking process with different initial longitudinal velocities.

Remark 6 (1) Although Refs. [6, 18–24] have simulated the vibration of non-longitudinal directions when the train runs at a constant longitudinal velocity, the simulation is only based on some local models and in a subset of all the six directions. While in this section, our simulation is based on a comprehensive dynamic model of the train and considers the coupling and feedback among the variables in all directions (see Section. 4.3), so the simulations in this section is closer to the real conditions. (2) There are still no relevant literatures simulating and analyzing the braking process

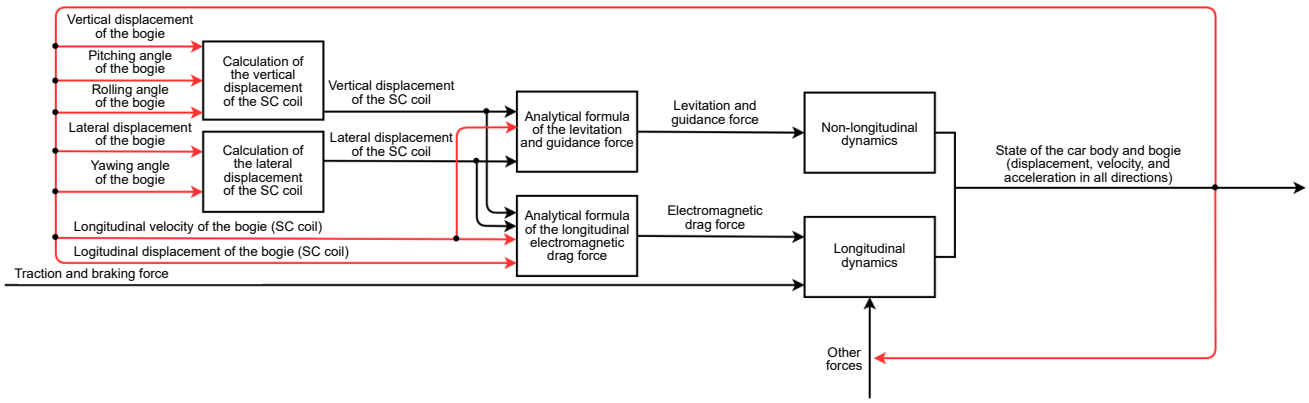

Fig. 4 System diagram of the comprehensive model for the SC-EDS train.

Table 2 Parameters of MLX01.

Parameter	Value
Weight of the bogie m_b	6×10^3 kg
Weight of the car body m_c	1.4×10^4 kg
Stiffness of the vertical air spring k_z	2×10^5 N·m^{-1}
Vertical damping coefficient c_z	5×10^3 N·s·m^{-1}
Stiffness of the lateral air spring k_y	1×10^5 N·m^{-1}
Lateral damping coefficient c_y	3×10^3 N·s·m^{-1}
Longitudinal length of the ground coil L_1	0.35 m
Vertical length of the ground coil L_2	0.34 m
Longitudinal length of the SC coil $2l_1$	1.07 m
Vertical length of the SC coil $2l_2$	0.5 m
Pole pitch of the ground coil $\tau/3$	0.45 m
Pole pitch of the SC coil τ	1.35 m
Turns of the ground coil N_1	24
Turns of the SC coil N_2	1400
Vertical distance between the center of upper and lower loops	0.42 m
Lateral distance between the center of ground coil and SC coil	0.185 m

of the SC-EDS train.

5.2 Simulation results and analysis

(1) Scenario 1

In this scenario, we mainly test the vibrations of the train in vertical direction when it runs with a constant longitudinal speed of 120 m/s but with different initial bogie heights, which are selected from the interval $[-0.2, 0.2]$ m. It is worth noting that among the various settings, the difference between the bogie height and the car body height is fixed, considering that the air springs between the car body and the bogie are compressed by the weight of the car body in the initial states, so once the initial bogie height is given, the corresponding initial car body height is also determined.

Table 3 summarizes the simulation results for all different initial heights, from which we have the following conclusions: (1) When the initial height of the bogie is within the interval $[-0.172, 0.113]$ m, the system can reach the steady state from the initial state; (2) A closer difference between the initial and final steady state values of the bogie height means a smaller fluctuation in the transition process; (3) When the initial height of the bogie is too high or too low (i.e., exceeds the interval $[-0.172, 0.113]$ m in this example), the system cannot reach the steady state.

Table 3 Simulation results for all different initial heights.

Initial height of the bogie $z_{b,10}$ (m)	Whether system can reach steady state normally	Fluctuation in the transition process
$z_{b,10} \leqslant -0.172$	No	−
$-0.172 \leqslant z_{b,10} \leqslant 0.113$	Yes	A smaller difference between $z_{b,10}$ and the steady state corresponding to a smaller fluctuation amplitude
$z_{b,10} \geqslant 0.113$	No	−

Figure 5 further shows the vertical and lateral displacements of the bogie and car body with the initial bogie heights of 0 m, −0.002 m, and −0.004 m, from which we can observe the above conclusions more intuitively. It can be seen that the vertical displacements (heights) of the car body and bogie are significantly affected by the initial height, but we can hardly find the differences among the lateral displacements corresponding to different initial heights.

The simulation results in this scenario have the following guiding significance for the height design of landing gear (supporting wheel) of the SC-EDS train in practice: (1) Since the height of the landing gear equals to the initial bogie height, the height of the landing gear must be within the height interval that guarantees a steady state; (2) The difference between the height of the landing gear and the steady-state height of the bogie could be selected small enough to reduce the fluctuation in the transition process and improve the comfort of passengers. It is noted that we have also tested different longitudinal running velocities other than 120 m/s and observed their influences on vertical and lateral displacements. The results are not given here due to the space limitation.

(2) Scenario 2

In this scenario, we mainly test the vibrations of the train in lateral direction when it runs with a constant longitudinal speed of 120 m/s but with different stiffness of lateral air springs in the interval $[0, 5\times10^5]$ N·m^{-1} and different lateral damping coefficients in the interval $[0, 5\times10^3]$ N·s·m^{-1}.

Table 4 summarizes the simulation results for all parameter settings of the lateral air springs and the lateral damping, from which we have the following conclusions: (1) The lateral vibration of the train is affected by both the stiffness of the lateral air springs and the damping coefficient; (2) When the lateral damping coefficient is fixed, increasing the stiffness of the lateral air springs but within a certain range (i.e., $[0, 2.18\times10^5]$ N·m^{-1} in this example) may lead to

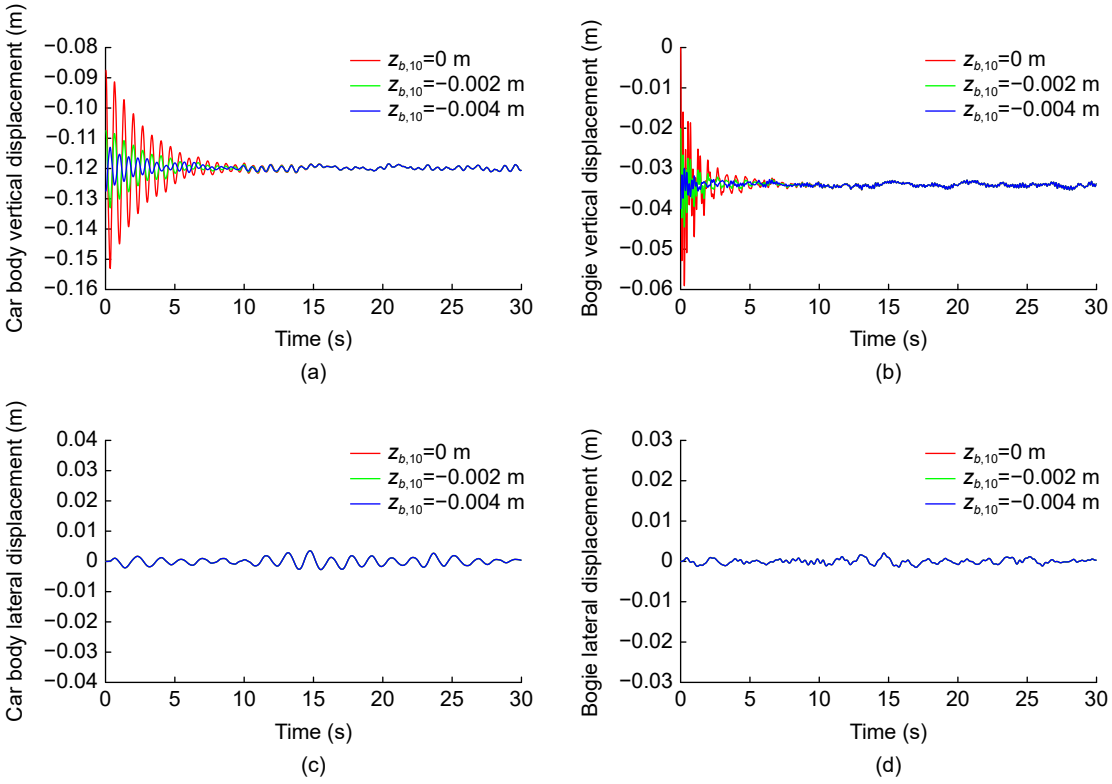

Fig. 5 Simulation results for three different initial heights.

Table 4 Simulation results for all parameter settings of the lateral air springs and damping.

Stiffness of the lateral air springs k_y ($\mathrm{N\cdot m^{-1}}$)	Lateral damping coefficient c_y ($\mathrm{N\cdot s\cdot m^{-1}}$)	State of the system	Fluctuation
$k_y \leqslant 2.18\times10^5$	Fixed at 3×10^3	Fluctuating around the steady state	A smaller k_y corresponds to a smaller fluctuation
$k_y \geqslant 2.18\times10^5$	Fixed at 3×10^3	Divergence	–
Fixed at 1×10^5	$c_y \leqslant 1.02\times10^3$	Divergence	–
Fixed at 1×10^5	$c_y \geqslant 1.02\times10^3$	Fluctuating around the steady state	A larger c_y corresponds to a smaller fluctuation

higher lateral vibration of both the car body and the bogie, and if the stiffness of the lateral air springs is too large (i.e., exceeds $[0, 2.18\times10^5]\ \mathrm{N\cdot m^{-1}}$), the vibration may diverge; (3) When the stiffness of the lateral air springs is fixed, increasing the lateral damping coefficient may lead to smaller lateral vibration of the car body and the bogie on one hand, but lead to some high-frequency harmonics on the other hand, and if the lateral damping coefficient is too small (i.e., exceeds $[1.02\times10^3, \infty]\ \mathrm{N\cdot s\cdot m^{-1}}$ in this example), the vibration may diverge.

Figures 6 and 7 further show three examples of the lateral displacements of the bogie and car body. It can be seen from Fig. 6 that when the stiffness of the lateral air springs is $4\times10^5\ \mathrm{N\cdot m^{-1}}$, which exceeds the interval $[0, 2.18\times10^5]\ \mathrm{N\cdot m^{-1}}$, the vibration is diverging. While from Figs. 6 and 7, it is clear that decreasing the stiffness of the lateral air springs and increasing the lateral damping coefficient lead to smaller lateral vibration on one hand but lead to some high-frequency harmonics on the other hand.

In real applications, in order to improve the comfort of passengers, it is necessary to reduce the vibration of the car body as much as possible. The above analysis reminds us to reduce the stiffness of the lateral air springs and increase the lateral damping coefficient. However, if the lateral damping coefficient is selected too large, the high frequency harmonics may occur in the vibration of the bogie. These may increase the risk of failure of the on-board SC coils and other equipment. Similar problem may also exist for the vertical vibration of the car body and bogie. So in practice, the above factors should be considered comprehensively, and besides adjusting the stiffness of

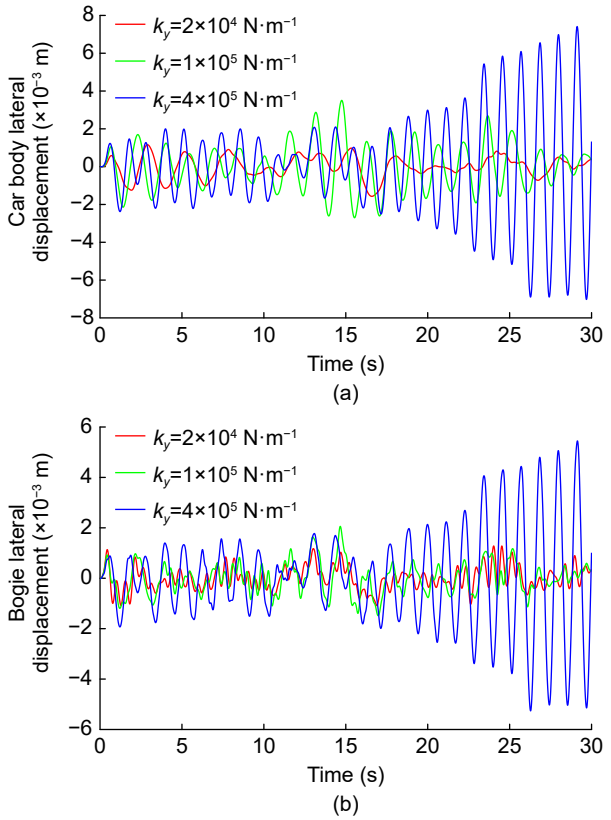

Fig. 6 Simulation results for three different settings of the lateral air springs stiffness.

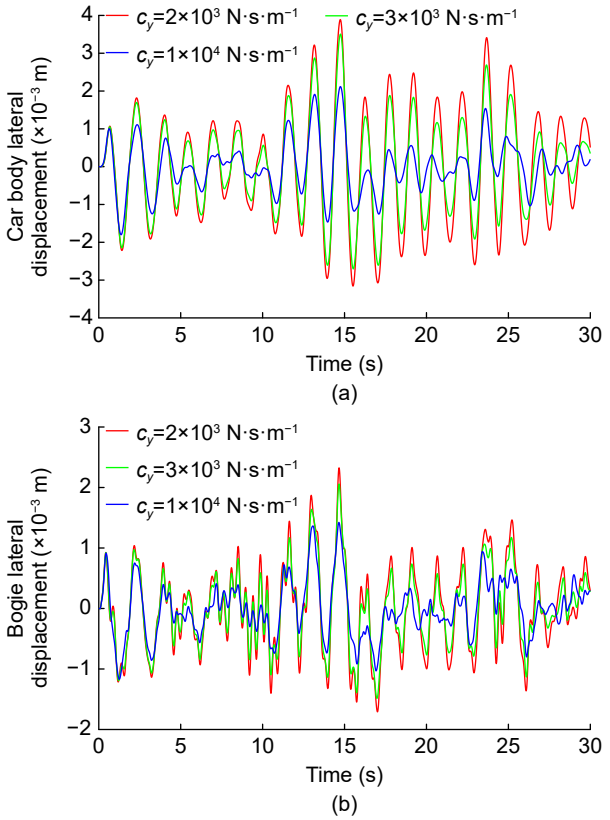

Fig. 7 Simulation results for three different settings of lateral damping coefficient.

air springs and damping coefficient, adding active controller can also be considered for vibration reduction[18, 19].

(3) Scenario 3

In this scenario, we test the motions and vibrations of the train in the suspension stage of the braking process with different initial longitudinal initial velocities.

Figures 8−10 show the simulation results of the motions and vibrations of the train in the suspension stage with initial longitudinal velocities of 120 m/s, 90 m/s, and 150 m/s, respectively.

From Figs. 8−10, it can be seen that the vertical displacement and vibration in the suspension stage of the braking process are affected by the initial velocity of the braking process. Decreasing the initial velocity leads to faster reduction of the vertical height of the car body and higher vibration. In practice, If the initial speed in the braking process is low, it is necessary to lower the landing gear earlier to enter the landing stage, otherwise vertical vibration will be aggravated and the vertical comfort of passengers will be reduced.

6 Conclusion

This paper builds a comprehensive model for the SC-EDS train, which considers the dynamics of the bogie and car body in all directions (including the longitudinal, vertical, lateral, pitching, rolling, and yawing directions). Based on the model, a system diagram describing the complex coupling and feedback of the model is given. Further simulation of the motions of the train under three scenarios is carried out based on Matlab, which shows the potential use of the model in design of the SC-EDS train.

Although the model given in this paper is comprehensive in the sense that it involves all of the main components of the SC-EDS train (including car body, bogie, guideway, secondary suspension, SC coils, and ground coils), it is still different from the real SC-EDS train which usually has multiple car bodies and multiple bogies[6]. Besides, in spite of its effectiveness, mechanism Eq. (8) for calculating the traction force generated by the linear synchronous motor is a simplification of the real dynamics.

In the future, the model should be extended to involve multiple car bodies, multiple bogies, and more accurate mechanism formula for calculating the traction force. In addition, more comprehensive and reliable simulations can be carried out based on the model to observe and analyze the dynamics of the SC-

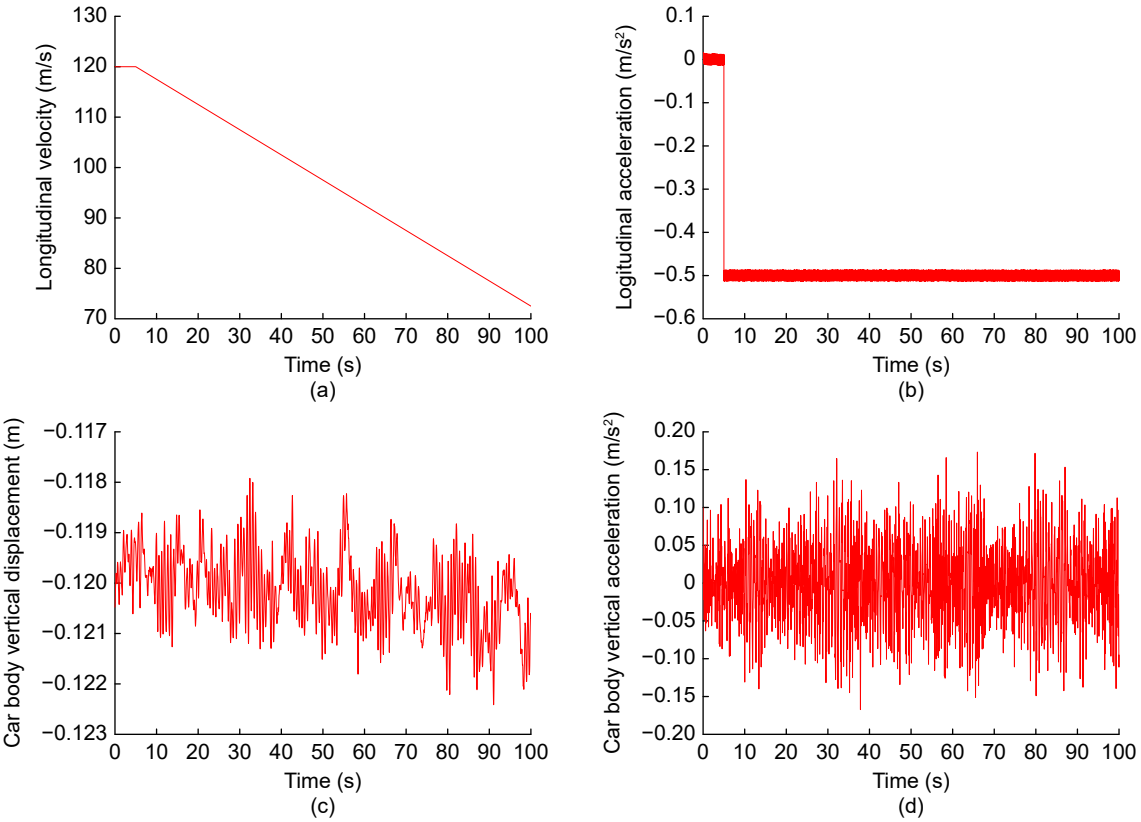

Fig. 8 Simulation results in the suspension stage of the braking process (initial velocity is 120 m/s).

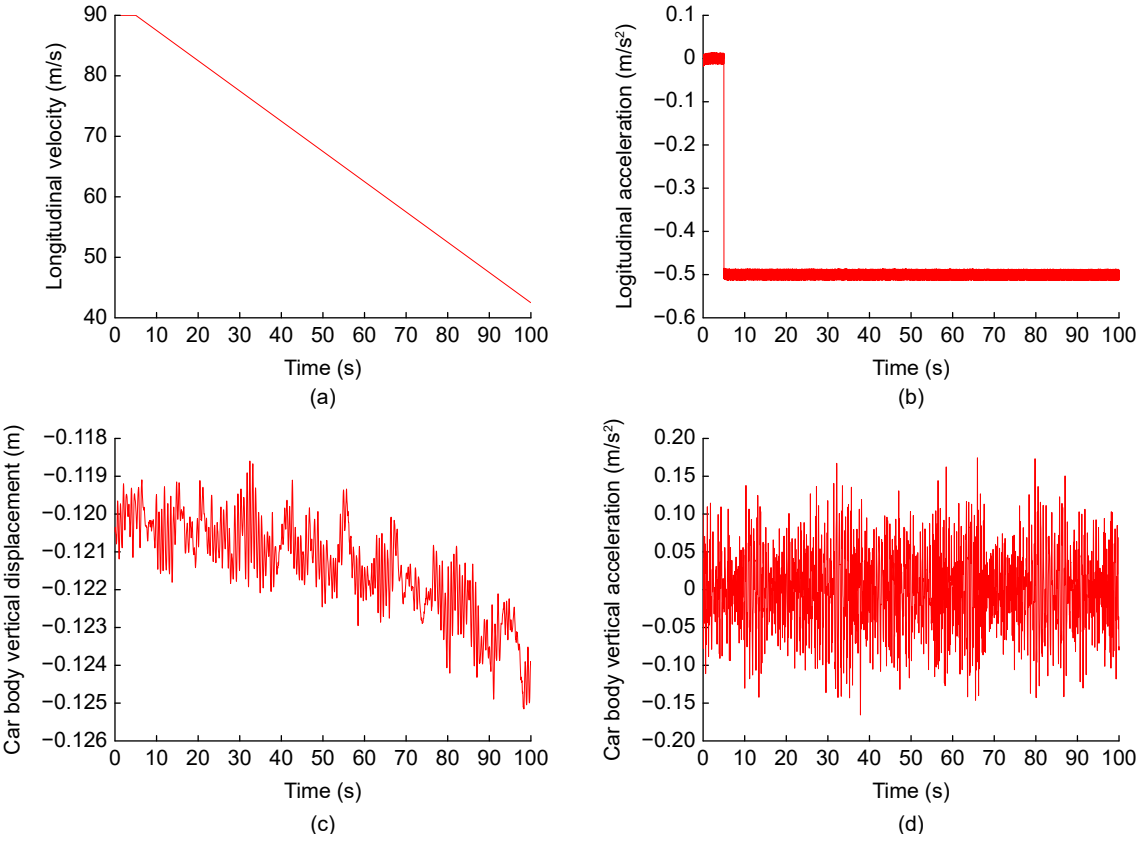

Fig. 9 Simulation results in the suspension stage of the braking process (initial velocity is 90 m/s).

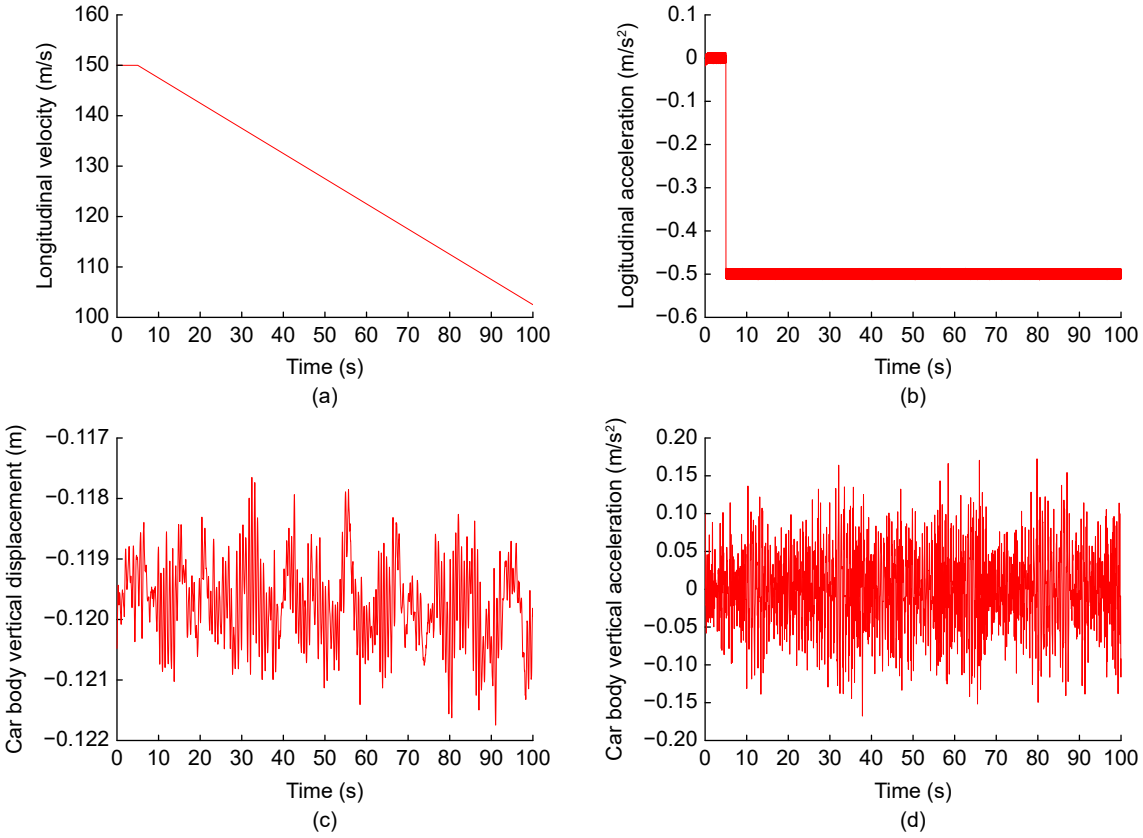

Fig. 10 Simulation results in the suspension stage of the braking process (initial velocity is 150 m/s).

EDS train, which may play a guiding role in designing the optimization and control strategies of vibration control, braking control, fault tolerant control, etc.

Acknowledgment

This work was supported by the Research and Development Project of CRSC Research and Design Institute Group Co., Ltd.

References

[1] L. Yan, Development and application of the maglev transportation system, *IEEE Trans. Appl. Supercond.*, vol. 18, no. 2, pp. 92–99, 2008.

[2] Z. Liu, Z. Long, and X. Li, *Maglev Trains: Key Underlying Technologies*. Heidelberg, Germany: Springer, 2015.

[3] J. Wang, S. Wang, J. Zheng, F. Yen, G. Ma, L. Liu, J. Li, and W. Liu, Recent developments of the high temperature superconducting maglev at ASCLab, *IEEE Trans. Appl. Supercond.*, vol. 21, no. 3, pp. 1551–1555, 2011.

[4] Y. Cai, G. Ma, Y. Wang, T. Gong, K. Liu, C. Yao, W. Yang, and J. Zeng, Semianalytical calculation of superconducting electrodynamic suspension train using figure-eight-shaped ground coil, *IEEE Trans. Appl. Supercond.*, vol. 30, no. 5, p. 3602509, 2020.

[5] J. Zhang, C. Zhao, Y. Feng, and X. Ren, Study on mechanical characteristics of the electrodynamic levitation and guidance system for the superconducting maglev train, (in Chinese), *Machinery*, vol. 47, no. 9, pp. 25–32, 2020.

[6] Z. Yan, G. Li, J. Luo, J. Zeng, W. Zhang, Y. Wang, W. Yang, and G. Ma, Vibration control of superconducting electro-dynamic suspension train with electromagnetic and sky-hook damping methods, *Veh. Syst. Dyn.*, vol. 60, no. 10, pp. 3375–3397, 2022.

[7] Central Japan Railway Company, http://English.Jr-central.Co.jp/company/ir/investor-meeting/pdf/im201603.Pdf, 2016.

[8] T. Yonezu, K. Watanabe, E. Suzuki, and T. Sasakawa, Study on electromagnetic force characteristics acting on levitation/guidance coils of a superconducting maglev vehicle system, *IEEE Trans. Magn.*, vol. 53, no. 11, p. 8300605, 2017.

[9] J. L. He, D. M. Rote, and H. T. Coffey, Electrodynamic forces of the cross-connected figure-eight null-flux coil suspension system, in *Proc. 13th Int. Conf. Magnetically Levitated Systems and Linear Drives*, Argonne, IL, USA, 1993, pp. 64–70.

[10] J. L. He, D. M. Rote, and H. T. Coffey, Applications of the dynamic circuit theory to maglev suspension systems, *IEEE Trans. Magn.*, vol. 29, no. 6, pp. 4153–4164, 1993.

[11] K. Davey, T. Morris, J. Shaaf, and D. Rote, Calculation of motion induced eddy current forces in null flux coils, *IEEE Trans. Magn.*, vol. 31, no. 6, pp. 4214–4216, 1995.

[12] J. He and H. T. Coffey, Magnetic damping forces in figure-eight-shaped null-flux coil suspension systems, *IEEE Trans. Magn.*, vol. 33, no. 5, pp. 4230–4232, 1997.

[13] S. Ohashi, H. Ohsaki, and E. Masada, Effect of the active damper coil system on the lateral displacement of the magnetically levitated bogie, *IEEE Trans. Magn.*, vol. 35, no. 5, pp. 4001–4003, 1999.
[14] S. Ohashi, Effect of the damper coils on the guideway displacement in the superconducting magnetically levitated bogie, *IEEE Trans. Appl. Supercond.*, vol. 22, no. 3, p. 3600604, 2012.
[15] S. Ohashi and T. Ueshima, Control method of the semi-active damper coil system in the superconducting magnetically levitated bogie against vertical and pitching oscillation, *IEEE Trans. Magn.*, vol. 48, no. 11, pp. 4542–4545, 2012.
[16] S. Ohashi and N. Ueda, Influence of the damper coil system on the levitation characteristics in the superconducting magnetically levitated system in case of SC coil quenching, *IEEE Trans. Magn.*, vol. 50, no. 11, p. 8300304, 2014.
[17] T. Okubo, N. Ueda, and S. Ohashi, Effective control method of the active damper system against the multidirectional vibration in the superconducting magnetically levitated bogie, *IEEE Trans. Appl. Supercond.*, vol. 26, no. 4, p. 3601804, 2016.
[18] K. Watanabe, H. Yoshioka, E. Watanabe, T. Tohtake, and M. Nagai, A study of the vibration control system for a superconducting maglev vehicle, in *Proc. 6th Int. Conf. Motion Vib. Control*, Saitama, Japan, 2002, pp. 907–912.
[19] K. Watanabe, H. Yoshioka, and E. Suzuki, Combined control of primary and secondary suspension of maglev vehicles, *Q. Rep. RTRI*, vol. 45, no. 1, pp. 26–31, 2004.
[20] J. Shirasaki, E. Suzuki, K. Watanabe, H. Hoshino, and M. Nagai, Improvement of vibration reduction performance of superconducting maglev vehicles using optimal preview control, (in Japanese), in *Proc. Dyn. Des. Conf.* , Higashi-Hiroshima, Japan, 2007, p. 410.
[21] K. Watanabe, H. Yoshioka, E. Suzuki, T. Tohtake, and M. Nagai, A study of vibration control systems for superconducting maglev vehicles (vibration control of lateral and rolling motions), *J. Syst. Des. Dyn.*, vol. 1, no. 3, pp. 593–604, 2007.
[22] K. Watanabe, H. Yoshioka, E. Suzuki, T. Tohtake, and M. Nagai, A study of vibration control systems for superconducting maglev vehicles (vibration control of vertical and pitching motions), *J. Syst. Des. Dyn.*, vol. 1, no. 4, pp. 703–713, 2007.
[23] E. Suzuki, J. Shirasaki, K. Watanabe, H. Hoshino, and M. Nagai, Comparison of methods to reduce vibrations in superconducting maglev vehicles by primary suspension control, *J. Mech. Syst. Transp. Logist.*, vol. 1, no. 1, pp. 3–13, 2008.
[24] H. Hoshino, E. Suzuki, and K. Watanabe, Reduction of vibrations in maglev vehicles using active primary and secondary suspension control, *Q. Rep. RTRI*, vol. 49, no. 2, pp. 113–118, 2008.
[25] P. Zhang, Optimal terminal iterative learning control for the parking control system of maglev train, *IOP Conf. Ser.: Earth Environ. Sci.*, vol. 587, no. 1, p. 012061, 2020.
[26] N. Nan, Y. Yang, W. Wei, W. Zhang, and Y. Liu, An operation control strategy of pull-in and departure station for medium-speed maglev train with battery constraints, in *Proc. 2018 37th Chinese Control Conference* (*CCC*), Wuhan, China, 2018, pp. 7810–7815.

Linfeng Liu received the BEng degree in automation from Tsinghua University, Beijing, China in 2020. He is currently pursuing the PhD degree in control science and engineering at Tsinghua University. His current research interests include optimization and control.

Hao Ye received the BEng and PhD degrees in automation from Tsinghua University, Beijing, China, in 1992 and 1996, respectively. He has been with the Department of Automation, Tsinghua University since 1996, where he is currently a professor. He is mainly interested in fault detection and diagnosis of dynamic systems.

Wei Dong received the BEng and PhD degrees from Tsinghua University, Beijing, China in 2000 and 2006, respectively. He is currently an associate research fellow with the Beijing National Research Center for Information Science and Technology, Tsinghua University. His main research interests include fault diagnosis, modeling, and simulation of complex engineering systems.

Junfeng Cui received the master degree in automation from Tsinghua University in 2006. Now he is working as a professor engineer in CRSC Research & Design Institute Group Co., Ltd. He has long been engaged in high-speed railway and high-speed maglev train operation control technology research.